Karamitros, D. K., Zoupantis, C., & Bouckovalas, G. D. (2016). Buried pipelines with bends: Analytical verification against permanent ground displacements. *Canadian Geotechnical Journal*, *53*(11), 1782-1793. https://doi.org/10.1139/cgj-2016-0060

Buried pipelines with bends: Analytical verification against permanent ground displacements

Dimitris K. Karamitros[1*], Christos Zoupantis[2], George D. Bouckovalas[3]

[1*] Lecturer in Civil Engineering

Faculty of Engineering, University of Bristol

Office 2.16, Queen's Building, University Walk, Clifton BS8 1TR, UK

Tel: +44 (0) 117 331 5701

E-mail: d.karamitros@bristol.ac.uk

[2] Civil Engineer, MSc

School of Civil Engineering, National Technical University of Athens

Heroon Polytechniou 9, Zografou 15780, Greece

E-mail: christos.zoupantis@gmail.com

[3] Professor

Geotechnical Department, School of Civil Engineering, National Technical University of Athens

Heroon Polytechniou 9, Zografou 15780, Greece

E-mail: gbouck@central.ntua.gr

Abstract

Available analytical methodologies for the stress analysis of buried pipelines against large permanent ground displacements (PGDs) apply only to straight pipeline segments. Hence, a new methodology is proposed herein for the analytical computation of pipeline strains in bends of arbitrary angle and radius of curvature, located outside the PGD high-curvature zone but within the pipeline's unanchored length. The methodology is based on the equivalent-linear analysis of the bend, assuming that it will perform as an elastic arched beam subjected to uniformly distributed ultimate axial and transverse horizontal soil reactions. The end of the bend towards the PGD zone is subjected to an axial displacement, calculated on the basis of overall displacement compatibility along the pipeline, while the other end is restrained by the unanchored pipeline segment beyond the bend. Using this approach, the maximum axial force at the vicinity of the PGD zone can be also calculated and consequently used for the estimation of the corresponding pipeline strains with any of the available numerical or analytical methodologies for straight pipeline segments. Parametric non-linear finite element analyses are performed in order to verify the analytical methodology and also derive conclusions of practical interest regarding the effect of bends on pipeline design.

Key Words

Pipelines, bends, permanent ground displacements, faults, analytical methodology.

1 Introduction

Permanent ground displacements (PGDs) are probably one of the most critical loading conditions that need to be taken into account in buried pipeline design (ALA-ASCE, 2005, O'Rourke & Liu, 2012). In earthquake-prone areas, such displacements are mainly associated with the rupture of active faults (e.g. Ha et al, 2008) or liquefaction-induced lateral spreading (e.g. O'Rourke et al, 2014). Nevertheless, they may also originate from more common geotechnical causes, such as slope failures (e.g. Cocchetti et al, 2009), underground works (e.g. Wang et al, 2011, Vorster et al, 2005, Marshall et al, 2010), differential settlement due to lowering of the groundwater table (e.g. Wols & van Thienen, 2014), differential heave of swelling soils (e.g. Rajeev & Kodikara, 2011) and differential frost heave (e.g. Hawlander et al, 2006). In all these cases, it is required to estimate the maximum developing pipeline strains and ensure that they remain below the allowable design limits (ALA-ASCE, 2005, EC8, 2006). The importance of accurate strain estimation and the appropriate prescription of remedial measures (i.e. use of thicker pipeline cross-section, selection of different backfill material, use of protective casing, or even alteration of the pipeline route) is not only driven from the crucial role of lifelines to support social and economic activity, but it is also dictated by the detrimental effects that may be manifested due to the leak of environmentally hazardous materials such as oil, gas or liquid waste.

A rigorous computation of pipeline strains requires the use of numerical analyses which take consistently into account the 3D geometry of the pipeline axis, the non-linear response of the pipeline steel and the surrounding backfill material, as well as second-order effects due to the applied large displacements (e.g. Xie et al, 2011, Vazouras et al, 2012). Nevertheless, pipeline response for medium and large applied displacements can become highly non-linear, thus the conduction of such analyses requires considerable expertise. Furthermore, taking into account the nature of pipelines as structures extending over large lengths, a significant number of analyses may be required along the pipeline route, while a time-consuming parametric investigation may be needed in cases where the required input (e.g. soil data) is not available. Therefore, for preliminary, at least, design purposes, engineers increasingly rely upon user-friendly

analytical solutions, which allow them to perform parametric analyses, identify critical locations and investigate the effectiveness of different remedial measures at a fraction of the time required for a consistent numerical investigation (e.g. Karamitros et al, 2007, 2011, Trifonov & Cherniy, 2010, 2012, Kouretzis et al, 2014). A common assumption of these analytical solutions is that the pipeline axis remains straight for a large distance away from the applied PGD zone. The only known exception is the analytical solution of O'Rourke & Liu (1999), which refers to the special case of pipelines with 90° elbows, under the simplifying assumptions that the arc-shaped geometry of the bend may be overlooked and that both the pipeline steel and the transverse soil resistance remain within the elastic range.

The present study aims to remedy the above limitations. More specifically, based on the equivalent-elastic beam theory, an analytical solution is presented for the stress analysis of pipelines with curved bends, for a wide range of bend angles, curvature radii, bend to PGD-zone distances and tensile permanent ground displacements. The bilinear stress-strain response of pipeline steel is taken into account through an iterative equivalent-linear solution scheme, while the Winkler-type soil springs are taken as elastic in the straight part of the pipeline and as perfectly plastic in the curved segment. Following a detailed presentation of the basic modeling assumptions and the analysis procedure, the accuracy of the analytical predictions is evaluated against the results of parametric 3D numerical analyses with the Finite Element Method.

2 Overview of analytical methodology

2.1 Basic assumptions

The basic geometrical characteristics of the problem analyzed herein are illustrated in Figure 1. Namely, a curved pipeline bend of angle φ with a radius of curvature R is located at a distance L_A from the point of PGD application on the pipeline axis. It is assumed that the bend lies outside the high-curvature zone which develops around the point of PGD application, but inside the pipeline's unanchored length, so that it will

affect the overall pipeline behavior. Simplified criteria to check L_A against the limiting distances resulting from the above requirements will be presented in following paragraphs.

The proposed methodology is based on the decomposition of the pipeline into a straight and a curved segment, based on endpoint A of the bend towards the PGD zone, as shown in Figure 2. Following this decomposition, analytical computations may be grouped in the following three basic sequential steps:

a. The 1st step focuses on the interaction between the bend and the applied PGD. More specifically, the axial displacement u_A of endpoint A of the bend is calculated as a function of the axial component Δx of the applied PGD, by imposing displacement compatibility along the straight segment of the pipeline shown in Figure 2b.
b. In the 2nd step, this displacement is applied to the curved part of the pipeline shown in Figure 2a and the resulting internal loads are calculated with the direct stiffness method, assuming that the bend behaves as an elastic arched beam. During this step, an equivalent secant Young's modulus is utilized for the pipeline steel and the analysis is performed iteratively, in order to take into account the associated non-linear response.
c. In the 3rd step, the axial force F_A and the displacement u_A at point A, computed from previous steps 1 and 2, are utilized to calculate the maximum axial force F_{max} developing in the point of PGD application. This is consequently implemented into existing analytical methodologies for straight pipeline segments to calculate the strains associated with the PGD zone. Alternatively, the bend can be replaced by an axial spring with stiffness $K_b=F_A/u_A$ and a numerical analysis can be performed, only focusing on the remaining straight segment and hence reducing the associated computational effort.

Taking into account that the axial displacement u_A derived from the 1st step depends also on the stiffness K_b of the bend which is computed in the 2nd step, it is realized that the 1st and 2nd steps above must be repeated until convergence is accomplished. In order to clarify this iterative procedure, a methodology workflow in presented in Appendix 2.

It should be emphasized that the present study refers exclusively to PGDs resulting in pipeline elongation, with tension being the prevailing mode of pipeline deformation. In cases where the applied PGD imposes compression to the pipeline (e.g. reverse faults), global pipeline buckling is possible and consequently the resulting strains should be estimated with detailed numerical analyses. Further than that, it is noted that the applied PGD may or may not follow a step-like deformation mode, as the detailed PGD distribution affects primarily the pipeline response in the adjacent high-curvature zone, while the response of the bend depends mostly on the component of the total displacement applied along the pipeline axis. Nevertheless, the assumption of step-like deformations, apart from being conservative for the overall pipeline verification, allows the proposed methodology to be directly combined with existing analytical solutions for the estimation of pipeline strains at the PGD zone, thus avoiding the use of additional more involved case-specific numerical analyses.

2.2 Limits of bend distance from the PGD zone

As mentioned earlier, the proposed methodology applies when the distance L_A of the bend from the PGD zone is (a) larger than the "pipeline curved length" L_c, i.e. the intensely curved length of the pipeline adjacent to the point of PGD application, and (b) smaller than the "pipeline unanchored length" L_{anch}, i.e. the distance from the point of PGD application to the point where relative pipeline-soil displacement becomes zero. This is because, for distances shorter than L_c, the simplifying assumptions of the methodology are not valid, while, for distances larger than L_{anch}, the presence of the bend becomes indifferent for pipeline verification. It is fortunate that the above distance limits can be readily estimated in terms of known in advance input parameters (i.e. the applied PGD, the pipeline characteristics and the ultimate soil reactions), before proceeding with the analytical computations.

More specifically, for large applied displacements, where the whole pipeline cross-section has undergone yielding, the "curved length" L_c on each side of the applied PGD may be geometrically approximated as (Kennedy et al, 1977):

$$L_c = \sqrt{2R_c\delta} \quad (1)$$

where R_c is the radius of curvature of the pipeline, estimated as:

$$R_c = \frac{F_{max}}{q_u} \quad (2)$$

In the above equations, F_{max} is the maximum axial force developing at the point of PGD application, q_u is the ultimate transverse soil resistance and δ is the component of the applied PGD perpendicular to the pipeline axis (Figure 3).

Taking into account that the methodology of Kennedy et al (1975) assumes complete yielding of the pipeline cross-section, F_{max} may be preliminarily estimated as the cross-sectional area of the pipe times the tensile yield strength of the pipeline steel. The remaining two parameters (δ and q_u) are defined in relation to the direction of the PGD. Namely, in the case of a lateral horizontal ground displacement Δh (e.g. at strike-slip fault crossings), the pipeline deforms symmetrically on both sides of the point of PGD application, so that $\delta=\Delta h/2$, while q_u corresponds to the ultimate soil resistance for lateral pipeline movement. In the case of vertical displacement Δv (e.g. normal faults), pipeline deformations are asymmetric, as the soil resistance to pipeline uplifting is significantly smaller than that for downward pipeline movement. Therefore, most of the applied vertical displacement is accommodated through pipeline uplifting over the hanging wall of the ground rupture, so that $\delta\approx\Delta v$, while q_u corresponds to the uplift resistance of the backfill soil. In either case, parametric application of the above equations indicates that for typical buried pipelines and applied PGDs, the curved length does not exceed a few tens of pipeline diameters.

In order to ensure that there is no interaction between the bend and the PGD zone, the minimum distance L_A should also include an additional attenuation length L_{att}, large enough to accommodate any significant pipeline deformations developing beyond the curved length L_c, as well as beyond the bend (i.e. to the right

of point A, in Figure 1). In other words, the minimum distance between the bend and the PGD zone should be larger than $L_A > L_c + L_{att}$. This attenuation length can be estimated by considering the equivalent problem of a laterally loaded single pile in elastic homogenous soil. Based on the analytical expression, by Karatzia and Mylonakis (2012), for the active length beyond which the behavior of a laterally loaded pile becomes independent of its length, Kouretzis et al (2014) estimated the attenuation length for the case of buried pipelines as $L_{tol} \approx 10D$, with D being the pipeline's diameter.

In general, ground displacements will impose a component Δx parallel to the pipeline axis, resulting in the development of tension or compression along the pipeline length. In the case of tension examined herein, the applied elongation Δx is accommodated through tensile strains along the "pipeline unanchored length" L_{anch} (Figure 3). For small and moderate applied elongations, where the axial force on the pipeline does not exceed the corresponding yield strength, the unanchored length on each side of the PDG application point can be estimated as (Karamitros et al, 2007):

$$L_{anch} = \sqrt{\frac{E_1 A \Delta x}{t_u}} \tag{3}$$

where E_1 is the elastic Young's modulus of the pipeline steel, A is the pipeline's cross-section area and t_u is the ultimate friction between the pipeline and the surrounding soil. Parametric application of the above equation for typical buried pipelines indicates that the unanchored length is significantly larger than the corresponding curved length and may extend to several hundreds of pipeline diameters on each side of the ground rupture.

3 Analysis of the bend

The core of the proposed methodology is the structural analysis of the bend (i.e. the 2nd step referenced in Section 2.1), hence its presentation will precede that of the 1st and the 3rd steps of the methodology which have to do with the interaction between the bend and the PGD zone. More specifically, the pipeline bend is

analyzed as an elastic arched beam AB, subjected to an axial displacement u_A at the edge towards the PGD zone, as shown in Figure 4. Apart from $u_{A,}$ the beam is loaded with an axial uniformly distributed load t_u equal to the ultimate friction force applied by the surrounding soil, as well as a transverse load q_u, equal to the ultimate soil resistance for transverse horizontal pipeline displacement. Furthermore, rotational and transverse transitional springs are considered at both ends of the arch, while an additional axial spring is considered at end B.

The bend is subsequently solved using the direct stiffness method:

$$\{P\}-\{P_L\}=\left(\left[K\right]+\left[K_{spr}\right]\right)\{u\} \tag{4}$$

where $\{P\}=\{F_A\ Q_A\ M_A\ F_B\ Q_B\ M_B\}^T$ are the axial forces F, shear forces Q and bending moments M at the ends A and B of the beam, $\{P_L\}$ are the respective reaction forces corresponding to loads t_u and q_u, [K] is the (6×6) stiffness matrix of the arched beam, $[K_{spr}]$ is the (6×6) support springs matrix and $\{u\}=\{u_A\ v_A\ \varphi_A\ u_B\ v_B\ \varphi_B\}^T$ are the axial displacements u, the transverse displacements v and the rotations φ of endpoints A and B of the beam. The corresponding matrices are derived as follows.

Stiffness matrix K

Considering the curved beam's equilibrium, without the external loads t_u and q_u which are treated separately, yields:

$$\{P_B\}=\begin{Bmatrix}F_B\\Q_B\\M_B\end{Bmatrix}=\begin{bmatrix}\cos\varphi & \sin\varphi & 0\\-\sin\varphi & \cos\varphi & 0\\R(\cos\varphi-1) & R\sin\varphi & 1\end{bmatrix}\begin{Bmatrix}F_A\\Q_A\\M_A\end{Bmatrix}=[\Lambda]\{P_A\} \tag{5}$$

Therefore, the stiffness matrix [K] can be formed with the aid of the above transpose matrix [Λ]:

$$[K]=\begin{bmatrix} [F]^{-1} & \left([F]^{-1}\right)^{T}[\Lambda]^{T} \\ [\Lambda][F]^{-1} & [\Lambda]\left([F]^{-1}\right)^{T}[\Lambda]^{T} \end{bmatrix} \tag{6}$$

where [F] is the flexibility matrix of an arched beam, similar to the one examined herein, but with a fixed support at point B and with no supports at point A (Figure 5):

$$\{u_A\}=\begin{Bmatrix} u_A \\ v_A \\ \varphi_A \end{Bmatrix}=\begin{bmatrix} F_{11} & F_{12} & F_{13} \\ F_{21} & F_{22} & F_{23} \\ F_{31} & F_{32} & F_{33} \end{bmatrix}\begin{Bmatrix} F_A \\ Q_A \\ M_A \end{Bmatrix}=[F]\{P_A\} \tag{7}$$

The elements of the flexibility matrix can be calculated using the principle of virtual work:

$$F_{ij}=\int_0^{\varphi}\frac{M_i(\theta)\cdot M_j(\theta)}{EI}Rd\theta \tag{8}$$

where E is the Young's modulus of the pipeline steel, I is the second moment of area of the pipeline cross section and $M_i(\theta)$ is the bending moment distribution along the curved beam, for an applied unit axial force (i=1), shear force (i=2) and moment (i=3) at end A (Figures 5a to c). More specifically:

$$M_1(\theta)=R(\cos\theta-1) \tag{9a}$$

$$M_2(\theta)=R\sin\theta \tag{9b}$$

$$M_3(\theta)=1 \tag{9c}$$

Therefore:

$$[F]=\begin{bmatrix} \frac{R^3}{EI}\left(\frac{3\varphi}{2}+\frac{\sin 2\varphi}{4}-2\sin\varphi\right) & \frac{R^3}{EI}\left(\cos\varphi-\frac{\cos 2\varphi}{4}-\frac{3}{4}\right) & \frac{R^2}{EI}(\sin\varphi-\varphi) \\ & \frac{R^3}{EI}\left(\frac{\varphi}{2}-\frac{\sin 2\varphi}{4}\right) & \frac{R^2}{EI}(1-\cos\varphi) \\ \text{(symmetric)} & & \frac{R}{EI}\varphi \end{bmatrix} \tag{10}$$

Reaction force matrix P_L

Considering the same arched cantilever beam with a fixed support at point B (Figure 5d), the reactions to the applied soil friction forces t_u and the transverse soil resistance forces q_u may be calculated using equations of equilibrium:

$$\{P_{BL}\}=\begin{Bmatrix} F_{BL} \\ Q_{BL} \\ M_{BL} \end{Bmatrix}=\begin{Bmatrix} Rq_u(1-\cos\varphi)-Rt_u\sin\varphi \\ Rq_u\sin\varphi+Rt_u(1-\cos\varphi) \\ R^2q_u(1-\cos\varphi)+R^2t_u(\varphi-\sin\varphi) \end{Bmatrix} \tag{11}$$

The bending moment distribution due to the applied soil reaction forces may be derived by substituting φ with θ, in the above equation:

$$M_L=R^2t_u(\theta-\sin\theta)+R^2q_u(1-\cos\theta) \tag{12}$$

Hence, using Equations 9 and 12, the corresponding axial displacement (i=1), transverse displacement (i=2) and rotation (i=3) of point A may be calculated, based on the principle of virtual work, as:

$$\Delta_{AL,i}=\int_0^{\varphi}\frac{M_i(\theta)\cdot M_L(\theta)}{EI}Rd\theta \tag{13}$$

Finally:

$$\{\Delta_{AL}\}=\begin{Bmatrix} u_{AL} \\ v_{AL} \\ \varphi_{AL} \end{Bmatrix}=\frac{R^3}{EI}\cdot\begin{Bmatrix} t_uR\left(\varphi\sin\varphi-\frac{\varphi^2}{2}-\frac{\sin^2\varphi}{2}\right)+q_uR\left(2\sin\varphi-\frac{\sin2\varphi}{4}-\frac{3\varphi}{2}\right) \\ t_uR\left(\sin\varphi-\varphi\cos\varphi-\frac{\varphi}{2}+\frac{\sin2\varphi}{4}\right)+q_uR\left(1-\cos\varphi-\frac{\sin^2\varphi}{2}\right) \\ t_u\left(\frac{\varphi^2}{2}+\cos\varphi-1\right)+q_u(\varphi-\sin\varphi) \end{Bmatrix} \tag{14}$$

Utilizing the above matrix, in combination with [F] and [Λ], the reaction matrix $\{P_L\}$ may be formed:

$$\{P_L\} = \begin{Bmatrix} -[F]^{-1}\{\Delta_{AL}\} \\ \{P_{BL}\} - [\Lambda][F]^{-1}\{\Delta_{AL}\} \end{Bmatrix} \quad (15)$$

Note that in the Direct Stiffness Method, the opposite of this matrix (i.e. -{P_L}) is applied to the beam as a loading, as indicated by Equation 4.

Support springs matrix $K_{springs}$

The constants of the transverse and rotational springs supporting edges A and B of the examined arched beam are calculated assuming that the pipeline away from the bend is behaving as a semi-infinite elastic beam on elastic foundation, with a Winkler-type spring constant equal to k (Figure 6). Therefore, the elastic line w(x) away from A and B may be described from the following differential equation:

$$E_1 I \frac{d^4 w}{dx^4} + kw = 0 \quad (16)$$

Solving the above under the condition that w(x)→0 when x→∞ yields:

$$w = e^{-\lambda x} C_1 \sin\lambda x + e^{-\lambda x} C_2 \cos\lambda x \quad (17a)$$

where:

$$\lambda = \sqrt[4]{\frac{k}{4E_1 I}} \quad (17b)$$

Following the positive sign convention for point A (Figure 6a), it is u=w, φ=w′, M=-EIw′′ and Q=EIw′′′, thus the following boundary conditions may be derived for point A:

$$Q_A = Q(0) = 4E_1 I\lambda^3 w(0) + 2E_1 I\lambda^2 w'(0) = 4E_1 I\lambda^3 u_A + 2E_1 I\lambda^2 \varphi_A \quad (18a)$$

$$M_A = M(0) = 2E_1 I\lambda^2 w(0) + 2E_1 I\lambda w'(0) = 2E_1 I\lambda^2 u_A + 2E_1 I\lambda \varphi_A \quad (18b)$$

For point B (Figure 6b), it is u=w, φ=-w′, M=EIw′′ and Q=EIw′′′, thus the corresponding boundary conditions become:

$$Q_B = Q(0) = 4E_1I\lambda^3 w(0) + 2E_1I\lambda^2 w'(0) = 4E_1I\lambda^3 u_B - 2E_1I\lambda^2 \varphi_B \quad (19a)$$

$$M_B = M(0) = -2E_1I\lambda^2 w(0) - 2E_1I\lambda w'(0) = -2E_1I\lambda^2 u_B + 2E_1I\lambda \varphi_B \quad (19b)$$

Equations 18 and 19 essentially provide the spring constants for the rotational and translational spring supports. It should be noted that in both sets of equations the shear forces and bending moments are coupled with respect to displacements and rotations, hence the spring matrix will contain non-zero elements outside the main diagonal.

The constant of the axial spring at end B of the arched beam is calculated by examining the axial stress and strain distribution in the straight part of the pipeline, beyond the bend. More specifically, as shown in Figure 7, the axial force developing in this part of the pipeline is linearly decreasing with the distance from point B, due to the constant friction force t_u applied by the surrounding soil, and becomes zero at a distance $L_{B,anch}=F_B/t_u$. The elongation of this part of the pipeline can be calculated by considering elastic behavior for the pipeline steel and integrating the strains along its length:

$$u_B = \int_0^{L_{B,anch}} \frac{F_B - t_u x}{E_1 A} dx = \frac{F_B^{\,2}}{2E_1 A t_u} \quad (20)$$

The constant for the axial spring at node B may be therefore calculated as:

$$k_{u,B} = \frac{F_B}{u_B} = \frac{2E_1 A t_u}{F_B} \quad (21)$$

It should be observed that the above constant is a function of the axial force at point B, which is not a priori known. Nevertheless, application of the proposed algorithm indicated that the variation of axial forces along

the bend is rather small, hence the axial force F_A at point A can be utilized instead of F_B, with minor effect on the final results.

Summarizing the above, the spring matrix is constructed as follows:

$$[K_{springs}]=\begin{bmatrix} 0 & 0 & 0 & 0 & 0 & 0 \\ 0 & 4E_1I\lambda^3 & 2E_1I\lambda^2 & 0 & 0 & 0 \\ 0 & 2E_1I\lambda^2 & 2E_1I\lambda & 0 & 0 & 0 \\ 0 & 0 & 0 & 2E_1At_u/F_A & 0 & 0 \\ 0 & 0 & 0 & 0 & 4E_1I\lambda^3 & -2E_1I\lambda^2 \\ 0 & 0 & 0 & 0 & -2E_1I\lambda^2 & 2E_1I\lambda \end{bmatrix} \tag{22}$$

System solution

Finally, the following system of equations is derived:

$$\{P\}-\{P_L\}=\begin{Bmatrix}\{P_s\}_{1x1}\\ \{P_f\}_{5x1}\end{Bmatrix}=\begin{bmatrix}[K_{ss}]_{1x1} & [K_{sf}]_{1x5}\\ [K_{fs}]_{5x1} & [K_{ff}]_{5x5}\end{bmatrix}\begin{Bmatrix}\{u_s\}_{1x1}\\ \{u_f\}_{5x1}\end{Bmatrix}=\left([K]+[K_{spr}]\right)\{u\} \tag{23}$$

In the above equation, the stiffness matrix is the sum $[K]+[K_{springs}]$, with no additional rearrangement being required. The known quantities are the applied displacement at end A, namely $\{u_s\}=u_A$ and the forces $\{P_f\}=\{Q_A\ M_A\ F_B\ Q_B\ M_B\}^T$, which are opposite to the corresponding internal reaction forces $-\{P_L\}$. The unknown quantities are the axial force at node A, namely $\{P_s\}=F_A$, and the displacements $\{u_f\}=\{v_A\ \varphi_A\ u_B\ v_B\ \varphi_B\}^T$. These are calculated as follows:

$$\{u_f\}=[K_{ff}]^{-1}\left(\{P_f\}-[K_{fs}]\{u_s\}\right) \tag{24a}$$

$$\{P_s\}=[K_{ss}]\{u_s\}+[K_{sf}]\{u_f\} \tag{24b}$$

In order to calculate the internal forces at the ends of the beam, the reaction force matrix needs to be re-added and the spring forces to be subtracted:

$$\{P\} = \begin{Bmatrix} \{P_s\} \\ \{P_f\} \end{Bmatrix} + \{P_L\} - \left[K_{springs}\right] \begin{Bmatrix} \{u_s\} \\ \{u_f\} \end{Bmatrix} \tag{25}$$

The distribution of axial forces F(θ), shear forces Q(θ) and bending moments M(θ) can be consequently derived as:

$$F(\theta) = F_A \cos\theta + Q_A \sin\theta + R q_u (1 - \cos\theta) - R t_u \sin\theta \tag{26a}$$

$$Q(\theta) = -F_A \sin\theta + Q_A \cos\theta + R q_u \sin\varphi + R t_u (1 - \cos\varphi) \tag{26b}$$

$$M(\theta) = F_A R(\cos\theta - 1) + Q_A R \sin\theta + M_A + R^2 q_u (1 - \cos\theta) + R^2 t_u (\theta - \sin\theta) \tag{26c}$$

Non-linear behavior of pipeline steel

In the previously presented solution, the pipeline was considered to behave elastically. To account for the non-linear behavior of the pipeline steel, the above procedure is applied iteratively, using an equivalent secant Young's modulus E′ for the pipeline steel, until compatibility is achieved between the stresses and strains developing on the pipeline, at the position of maximum bending moment M_{max}. It is noted that the negative bending moments calculated for endpoints A and B of the bend may exceed in absolute value the maximum positive bending moment developing in the middle of the bend. Nevertheless, this is attributed to the stiffness of the support springs, which have been calculated under the conservative assumption that the Winkler-type soil springs away from the bend behave elastically. In reality, for large displacements and rotations of points A and B, the ultimate transverse soil resistance will be reached even beyond the ends of the bend. This will result in an increase of the overall flexibility of the bend and a reduction of the developing axial forces and bending moments along the pipeline. In order to remain conservative, the proposed methodology maintains the assumption of elastic support springs for the bend. However, it is recommended that the bending moments at endpoints A and B are not taken into account and M_{max} is taken as the maximum positive bending moment.

The procedure adopted for the calculation of E´ is the same as that initially proposed by Karamitros et al (2007, 2011), and subsequently adopted by Trifonov & Cherniy (2010, 2012). The basic equations of the corresponding algorithm are repeated herein as Appendix 1, in order to enable independent reading of the paper.

4 Interaction between PGD zone and pipeline bend

4.1 Displacement Compatibility

The first element of the interaction between the PGD zone and the pipeline bend is related to the computation of the axial displacement u_A applied at endpoint A of the bend (i.e. the 1st step referred to in Section 2.1). This is achieved by considering compatibility of displacements between the axial component Δx of the applied PGD, the displacement u_A at the beginning of the bend, as well as the elongation ΔL of the straight segment of the pipeline:

$$\Delta x = \Delta L + u_A \tag{27}$$

The elongation ΔL is calculated by integrating the axial strains developing along the straight part of the pipeline. The corresponding strain distribution is determined by assuming an elastic stress-strain behavior for the pipeline steel, as well as a linear distribution of axial forces along the pipeline's length, due to a fully mobilized friction force t_u applied by the surrounding soil. More specifically, as shown in Figure 8, the axial force increases from F_A at endpoint A of the bend, to $F_{max}=F_A+t_uL_A$ at the PGD point of application, and subsequently decreases to F=0 at a distance $L_{anch}=F_{max}/t_u$. According to the above:

$$\Delta L = \int_0^{L_A} \frac{F_A + t_u x}{E_1 A} dx + \int_0^{L_{anch}} \frac{F_{max} - t_u x}{E_1 A} dx = \frac{1}{E_1 A}\left(\frac{F_A^{\,2}}{2t_u} + 2L_A F_A + t_u L_A^{\,2}\right) \tag{28}$$

The axial force F_A applied to the end of the bend may be correlated to the corresponding displacement u_A through a stiffness coefficient K_b, as $F_A=K_b u_A$. In this case, Equations 27 and 28 yield:

$$u_A = \frac{-E_1 A t_u - 2L_A K_b t_u + \sqrt{\left(E_1 A t_u\right)^2 + 2\left(L_A K_b t_u\right)^2 + 4E_1 A L_A K_b t_u{}^2 + 2E_1 A K_b{}^2 t_u \Delta x}}{K_b{}^2} \tag{29}$$

The stiffness K_b in Equation 29 is not known before analyzing the bend. Therefore, an initial displacement $u_{A,o}$ is applied to the end of the bend and the reaction F_A is consequently determined. K_b is redefined as F_A/u_A and the procedure is repeated until convergence (in terms of either K_b, u_A or F_A) is achieved.

The displacement $u_{A,o}$ used in the first iteration can be defined as the displacement of the same point A (i.e. at a distance L_A from the PGD location), while assuming that no bend exists in the pipeline route. In that case, the displacement compatibility equation would become:

$$\Delta x = 2 \cdot \int_0^{L_{anch}} \frac{F_{max} - t_u x}{E_1 A} dx = \frac{F_{max}{}^2}{E_1 A t_u} \tag{30}$$

Therefore, the axial force $F_{A,o}$ at a distance L_A would be equal to:

$$F_{A,o} = F_{max} - t_u L_A = \sqrt{E_1 A t_u \Delta x} - t_u L_A \tag{31}$$

and the corresponding displacement would be equal to the integral of axial strains further away from this point, as:

$$u_{A,o} = \int_0^{F_{A,o}/t_u} \frac{F_{A,o} - t_u x}{E_1 A} dx = \frac{F_{A,o}{}^2}{2E_1 A t_u} \tag{32}$$

It is acknowledged that the above derivation is only valid when the axial strains along the straight segment of the pipeline remain elastic. Therefore, the proposed methodology is applicable only when:

$$F_{max} = F_A + t_u L_A < \sigma_1 A \tag{33}$$

where σ_1 is the yield stress of the pipeline steel.

4.2 Pipeline verification at the PGD zone

The second element of the interaction between the PGD zone and the pipeline bend is related to the computation of the pipeline stresses and strains in the vicinity of the application point of the PGD (i.e. the 3rd step referred to in Section 2.1). More specifically, following the convergence of Steps 1 and 2 of the proposed methodology, the displacement u_A and axial force F_A at the beginning of the bend are determined and can be consequently employed for the analysis of the pipeline at the PGD zone. Depending on the required level of accuracy, there are two ways to accomplish that, as described below:

a. Many of the currently available analytical methodologies for the strength verification of buried pipelines against step-like PGDs (e.g. Karamitros et al, 2007, 2012 and Trivonov & Cherniy, 2011, 2012, for fault crossings, or Kouretzis et al, 2014, for differential settlement or heave) provide estimations of the corresponding design strains as a function of the maximum axial force F_{max} developing at the point of PGD application. In these methodologies, F_{max} is calculated assuming a straight pipeline route. Nevertheless, having calculated the axial force F_A at endpoint A of the bend, the axial force F_{max} can be readily estimated as $F_A+t_uL_A$ and subsequently incorporated into the same methodologies, in order to quantify the effect of the bend on the pipeline behavior at the PGD zone.
b. If the strains developing near the PGD zone are critical for pipeline design, a more detailed numerical analysis may be required. An accurate simulation of the pipeline bend in this case might result in complicated meshes that require a lot of time and expertise to be created. Nevertheless, this can be avoided by replacing the bend with an elastic axial spring, featuring a stiffness of $K_b=F_A/u_A$. This would introduce the effect of the bend on pipeline performance, while significantly reducing the overall computational effort.

5. Evaluation of proposed methodology

The accuracy of the proposed methodology was evaluated through comparison with numerical predictions from parametric analyses with the Finite Element Method and the commercial code ANSYS 12 (ANSYS Inc., 2009). A typical high-pressure natural gas pipeline was considered for this purpose, featuring an external diameter of D=0.9144m (36") and a wall thickness of t=0.0119m. The pipe was made of API5L-X65 carbon steel, the behavior of which was described by a bi-linear stress-strain relationship, with the properties listed in Table 1. The pipeline route included a bend of angle φ, which varied parametrically from 0° (straight axis) to 90°, with a radius of curvature R, which similarly varied from 5D to 40D. The pipeline was discretized in 0.50m long elastoplastic beam elements, for a sufficient length on both sides of the point of PGD application, so that forces and displacements at the far ends diminish to zero.

To simulate soil-pipeline interaction, each node of the pipeline was connected to axial and transverse horizontal Winkler springs, modeled as elastic-perfectly plastic rod elements. The spring properties were calculated according to the ALA-ASCE (2005) guidelines, assuming that the pipeline is buried into silica sand backfill, with friction angle φ=36º and dry unit weight γ=18KN/m^2. A burial depth of 1.30m was considered, measured from the top of the pipe, resulting in the spring properties of Table 2. Since the applied ground displacements were horizontal, no vertical soil springs were utilized in the analyses and the corresponding degrees of freedom of the pipeline nodes were fixed.

The examined PGD involved a step-like movement of a seismic strike-slip fault, crossing the pipeline route at an angle of 45° and resulting in pipeline elongation. Fault displacements Δf of up to 2.0D were applied to the fixed end of the Winkler springs over the sliding wall of the fault, corresponding to a maximum axial Δx displacement of $\sqrt{2}$D. The distance L_A between the fault crossing and the bend was varied parametrically from 50D to 200D, as compared to the maximum estimated "pipeline curved length" $L_c \approx 10D$ and the maximum "pipeline unanchored length" $L_{anch} \approx 500D$.

The numerical and the analytical predictions are compared in the graphs of Figure 9, with each column of graphs focusing separately on the effects of the normalized bend distance L_A/D, the bend angle φ and the radius of curvature R/D, as well as of the normalized applied fault displacement Δf/D. Note that the parametric analyses compared in Figure 9 were performed with reference to a basic case with $L_A/D=100$, φ=45° and R/D=10. The first row of graphs refers to the maximum longitudinal pipeline strains developing at the bend ($\varepsilon_{max,bend}$), while the following two rows refer to the maximum strains developing in the vicinity of the fault crossing ($\varepsilon_{max,fault}$) and the maximum axial force developing at the fault trace (F_{max}). In addition, Figure 10 shows one-to-one comparisons for the above pipeline response measures, for the entire range of the input parameters. Note that the analytical predictions of $\varepsilon_{max,fault}$ in the above figures were obtained by combining the methodology proposed herein with the analytical solution of Karamitros et al (2007), for straight pipelines segments crossing strike-slip faults.

Examination of the maximum bend strains $\varepsilon_{max,bend}$, in the first row of graphs of Figure 9 reveals that they may become significant and may even surpass the corresponding strains at the PGD zone by an order of magnitude as the distance of the bend from the displacement zone decreases and the curvature characteristics of the bend become more intense, i.e. the bend angle φ increases and the radius of curvature R decreases. Furthermore, it is worth to observe that the most severe condition corresponds to intermediate bend angles φ=30-45^o and not to right bend angles φ=90^o, as it could be conventionally thought.

Focusing next on the pipeline strains and forces at the vicinity of the PGD zone, in the 2nd and 3rd rows of graphs in Figure 10, it is observed that there is a relatively minor effect from the presence of the bend which could be approximately overlooked. It is also interesting that the contribution of the bend was actually beneficial for bend angles φ>45^o, as the existence of the bend added flexibility to the system, resulting in reduced axial forces at the fault crossing. This is because a large part of the axial component of the applied displacement was undertaken by pipeline bending (at the curved part of the bend), instead of pipeline tension (at the straight part before the bend), as the bending stiffness EI of hollow cross-sections is considerably smaller than the corresponding axial stiffness EA. However, taking into account that the

overall stiffness also depends on soil reactions, it is speculated that this trend may be reversed for large transverse soil resistances (e.g. stiffer soil and/or larger burial depths) and small soil-pipe friction coefficients (e.g. when a pipeline liner is installed).

The analytical predictions capture the above trends with notable accuracy. In quantitative terms, for small and medium applied displacements, where the developing strains do not exceed 0.5%, the deviation between the analytically calculated maximum bend strains $\varepsilon_{max,bend}$ and the corresponding numerical results remains below 20%. Consistency is maintained for larger displacements, however the scatter gradually increases. This is attributed to the fact that large strains are associated with the formation of a plastic hinge within the bend, which cannot be accurately captured using an equivalent-linear approximation. A similar trend is observed for the maximum strains $\varepsilon_{max,fault}$ developing in the vicinity of the fault crossing. The methodology of Karamitros et al (2007) provides accurate estimations for small and medium strain levels of up to 0.5%. For larger deformations, where the pipeline behavior becomes highly non-linear, the corresponding strains are under-predicted by an average of 15%. Regarding the maximum axial force F_{max} developing at the fault trace, the proposed methodology consistently provides conservative estimations. This is due to the assumption of elastic support springs for endpoints A and B of the bend, which increase the overall stiffness of the system.

Finally, it is noted that some of the analytical predictions are omitted from Figures 9 and 10. For large normalized fault displacements Δf, large fault-bend distances L_A/D and small bending angles φ, this is because the analytically predicted F_{max} exceeded the yield strength of the pipeline, hence the assumption that the straight segment of the pipeline behaves elastically was no longer valid. In the case of smaller fault displacements $\Delta f/D$, small bending angles φ and large radii of curvature R/D, the bending moments developing at the bend became positive at endpoints A and B and negative in the middle, contrary to what was expected. This is attributed to the fact that the proposed methodology assumes mobilization of the ultimate transverse soil resistance along the arc AB, which is not realistic when the pipeline is almost

straight. Therefore, the proposed methodology should only be employed under the requirement that the computed M_A and M_B remain negative.

5 Concluding remarks

A simplified analytical methodology has been proposed, facilitating the stress analysis of buried pipelines against permanent ground displacements (PGDs), in the existence of a bend along the pipeline route. The methodology is applicable for PGDs resulting in pipeline elongation, with the bend being located within the pipeline unanchored length, yet outside the high-curvature zone adjacent to the application point of the PGD. It is acknowledged that during the presentation and verification of the proposed methodology, the flexibility of the bent part of the pipeline has been considered equal to that of a straight pipe. Even though this assumption is typical in many practical engineering applications, it should be clarified that the bending stiffness of curved thin-walled pipes can be significantly decreased due to the von Karman effect (e.g. Öry & Wilczek, 1983). However, this effect is diminished due to the pipeline's internal pressure (Bathe & Almeida, 1982) and the adjacency with straight segments (Thomas, 1981), while it may also be affected by the interaction with the surrounding soil. Nevertheless, in case that the user wishes to consider an increased flexibility for the curved part of pipeline, this can be readily performed in the proposed methodology, through an equivalent adjustment of the corresponding bending stiffness. Furthermore, it is acknowledged that the proposed methodology does not account for the effects of local buckling and section deformation and consequently its application should not be extended beyond the strain limits defined by design codes for such phenomena to be avoided.

Comparison between analytical predictions obtained with the proposed methodology and results from non-linear numerical analyses with the Finite Element Method indicated a good agreement for a wide range of the input parameters. Further than that, the parametric numerical and analytical predictions reviewed in this study revealed a number of practical conclusions with regard to the overall design of pipelines with bends against PGDs. In summary:

- Under the conditions stated above, the effect of bends on pipeline strains developing at the zone of the applied PGD is relatively minor and may be approximately overlooked. In the typical case examined herein, the effect of bend has proved even beneficial for bend angles $\varphi>45^{o}$, as a large part of the axial component of the applied displacement was undertaken by the bend and not by the straight pipeline segment in front of it.
- Nevertheless, pipeline strains at the bend may exceed the strains at the PGD zone, and become critical for the pipeline design. The difference may reach an order of magnitude, for bend angles $\varphi=30\text{-}45°$ and relatively small radii of curvature $R/D<20$.
- The assumption of 90^{o} bend angles is not always conservative, as it is commonly considered in practice.
- Large pipeline strains at bends may be efficiently mitigated by proper design of the pipeline routing. Namely, bends should be placed at a sufficiently large distance from the PGD zone, bend angles should be reduced below 30^{o} and radii of curvature should be increased above 15-20D.

Appendix 1

The procedure employed to take into account the bilinear stress-strain relationship of the pipeline steel (Figure 11) considers the exact distribution of stresses and strains on the pipeline's cross-section, as a function of the developing axial force and bending moment. More specifically, under the assumption that the deformed pipe section remains plane, the total longitudinal strain distribution can be expressed as:

$$\varepsilon(\beta) = \varepsilon_a + \varepsilon_b \cos\beta \tag{A1}$$

where β is the polar angle of the cross-section, defined in Figure 12, while ε_a and ε_b are the axial and bending strains, respectively. Bending strain ε_b is calculated from the maximum bending moment M_{max} as:

$$\varepsilon_b = \frac{M_{max} D}{2EI} \tag{A2}$$

The corresponding axial strain ε_a is calculated from the demand for the integral of stresses over the pipeline section to be equal to the developing axial force. For the sake of simplicity, the axial force F_A developing at point A can be utilized for this purpose. Considering the bilinear stress-strain relationship shown in Figure 11, the total stress distribution is given by:

$$\sigma(\beta)=\begin{cases}\sigma_1+E_2(\varepsilon-\varepsilon_1) & 0\le\beta<\beta_1\\ E_1\varepsilon & \beta_1\le\beta\le\pi-\beta_2\\ -\sigma_1+E_2(\varepsilon+\varepsilon_1) & \beta_2<\beta\le\pi\end{cases} \tag{A3}$$

where:

$$\beta_{1,2}=\begin{cases}\pi & \dfrac{\varepsilon_1\mp\varepsilon_a}{\varepsilon_b}<-1\\ \arccos\left(\dfrac{\varepsilon_1\mp\varepsilon_a}{\varepsilon_b}\right) & -1\le\dfrac{\varepsilon_1\mp\varepsilon_a}{\varepsilon_b}\le 1\\ 0 & \dfrac{\varepsilon_1\mp\varepsilon_a}{\varepsilon_b}<1\end{cases} \tag{A4}$$

The corresponding axial force is therefore derived as:

$$F=2\cdot\int_{\beta=0}^{\pi}\sigma\frac{D-t}{2}t\cdot d\beta=t(D-t)\begin{bmatrix}E_1\pi\varepsilon_a-(E_1-E_2)(\beta_1+\beta_2)\varepsilon_a\\ +(E_1-E_2)(\beta_1-\beta_2)\varepsilon_1\\ -(E_1-E_2)(\sin\beta_1-\sin\beta_2)\varepsilon_b\end{bmatrix} \tag{A5}$$

The axial strain ε_a that satisfies the requirement $F(\varepsilon_a)=F_A$ can be calculated iteratively, starting from $\varepsilon_a^o=0$ and utilizing the Newton-Raphson method, as follows:

$$\varepsilon_a^{k+1}=\varepsilon_a^k-\frac{F(\varepsilon_a^k)-F_a}{dF/d\varepsilon_a\Big|_{\varepsilon_a=\varepsilon_a^k}} \tag{A6a}$$

where:

$$\frac{dF}{d\varepsilon_a} = t(D-t)\left[\begin{array}{l} E_1\pi - (E_1-E_2)(\beta_1+\beta_2) - (E_1-E_2)\left(\frac{d\beta_1}{d\varepsilon_a}+\frac{d\beta_2}{d\varepsilon_a}\right)\varepsilon_a \\ +(E_1-E_2)\left(\frac{d\beta_1}{d\varepsilon_a}-\frac{d\beta_2}{d\varepsilon_a}\right)\varepsilon_1 - (E_1-E_2)\left(\frac{d\beta_1}{d\varepsilon_a}\cos\beta_1 - \frac{d\beta_2}{d\varepsilon_a}\cos\beta_2\right)\varepsilon_b \end{array}\right] \quad \text{(A6b)}$$

$$\frac{d\beta_{1,2}}{d\varepsilon_a} = \begin{cases} \pm\dfrac{1}{\varepsilon_b \sin\beta_{1,2}} & \varepsilon_b \sin\beta_{1,2} \le -0.01 \\ -100 & -0.01 < \varepsilon_b \sin\beta_{1,2} \le 0 \\ \pm 100 & 0 < \varepsilon_b \sin\beta_{1,2} \le 0.01 \\ \pm\dfrac{1}{\varepsilon_b \sin\beta_{1,2}} & 0.01 < \varepsilon_b \sin\beta_{1,2} \end{cases} \quad \text{(A6c)}$$

Note that the limits in Equation A6c have been arbitrarily introduced in order to accelerate the convergence procedure. The bending moment corresponding to ε_a and ε_b can be calculated as:

$$M = 2\int_{\beta=0}^{\pi}\sigma\left(\frac{D-t}{2}\right)^2 t\cos\beta\cdot d\beta = \\ = \frac{t(t-D)^2}{2}\left[\begin{array}{l} \dfrac{\pi E_1\varepsilon_b}{2} - (E_1-E_2)(\sin\beta_1 - \sin\beta_2)\varepsilon_a + (E_1-E_2)(\sin\beta_1+\sin\beta_2)\varepsilon_1 \\ -\dfrac{(E_1-E_2)(\beta_1+\beta_2)\varepsilon_b}{2} - \dfrac{(E_1-E_2)(\sin 2\beta_1+\sin 2\beta_2)\varepsilon_b}{4} \end{array}\right] \quad \text{(A7)}$$

This bending moment is not necessarily equal to the maximum developing bending moment M_{max} utilized in Equation A2. Therefore, in order to ensure compatibility between the applied force and bending moment and the corresponding developing axial and bending strains, an equivalent secant Young's modulus is estimated and the analysis of the bend (i.e. Step 2) is repeated until convergence is accomplished. The secant Young's modulus for the each subsequent iteration is calculated on the basis of moment M derived in Equation A7, as:

$$E' = \frac{MD}{2I\varepsilon_b} \quad \text{(A8)}$$

Appendix 2

In order to facilitate the practical application of the proposed methodololgy, a schematic workflow is presented in Figure 13.

References

1. ANSYS Inc. ANSYS release 12.0 documentation, 2009.
2. American Lifelines Alliance—ASCE (2005): "Guidelines for the Design of Buried Steel Pipe", July 2001 (with addenda through February 2005).
3. Bathe, K.J., Almeida, C.A. (1982): "Simple and effective pipe elbow element - Pressure stiffening effects", Journal of Applied Mechanics, Transactions ASME, 49 (4), pp. 914-916.
4. Cocchetti G, di Prisco C, Galli A. Soil–pipeline interaction along unstable slopes: a coupled three-dimensional approach. Part 2: Numerical analyses. Can Geotech J 2009;46:1305–21. doi:10.1139/T09-102.Karamitros, D.K., Bouckovalas, G.D., Kouretzis, G.P. 2007. Stress analysis of buried steel pipelines at strike-slip fault crossings, Soil Dynamics and Earthquake Engineering 27 (3), 200-211.
5. Comitee Europeen de Normalisation. Eurocode8: Design of structures for earthquake resistance, Part4: Silos, tanks and pipelines, CENEN1998-4, Brussels, Belgium, 2006.
6. Hawlader BC, Morgan V, Clark JI. Modelling of pipeline under differential frost heave considering post-peak reduction of uplift resistance in frozen soil. Can Geotech J 2006;43:282–93. doi:10.1139/t06-003.
7. Karamitros, D.K., Bouckovalas, G.D., Kouretzis, G.P., Gkesouli, V. 2011. An analytical method for strength verification of buried steel pipelines at normal fault crossings, Soil Dynamics and Earthquake Engineering 31 (11), 1452-1464.

8. Karatzia, X., and Mylonakis, G. 2012. Horizontal response of piles in inhomogeneous soil: Simple analysis. In Proceedings of the Second International Conference on Performance-Based Design in Earthquake Geotechnical Engineering, Taormina, Italy. Paper No. 1117.

9. Kennedy RP, Chow AW, Williamson RA. Fault movement effects on buried oil pipeline. Transport Eng J ASCE 1977;103:617–33.

10. Kouretzis GP, Karamitros DK, Sloan SW. Analysis of buried pipelines subjected to ground surface settlement and heave. Can Geotech J 2014:1–14. doi:10.1139/cgj-2014-0332.

11. Marshall AM, Klar A, Mair RJ. Tunneling beneath Buried Pipes: View of Soil Strain and Its Effect on Pipeline Behavior. J Geotech Geoenvironmental Eng 2010;136:1664–72. doi:10.1061/(ASCE)GT.1943-5606.0000390.

12. Newmark NM, Hall WJ. Pipeline design to resist large fault displacement. In: Proceedings of the US National Conference on Earthquake Engineering. Ann Arbor: University of Michigan; 1975. p. 416–25.

13. O'Rourke TD, Jeon S-S, Toprak S, Cubrinovski M, Hughes M, van Ballegooy S, et al. Earthquake Response of Underground Pipeline Networks in Christchurch, NZ. Earthq Spectra 2014;30:183–204. doi:10.1193/030413EQS062M.

14. O'Rourke MJ, Liu X. Response of buried pipelines subject to earthquake effects. Monograph Series, Multidisciplinary Center for Earthquake Engineering Research (MCEER); 1999.

15. O'Rourke MJ, Liu JX. Seismic Design of Buried and Offshore Pipelines. Multidisciplinary Center for Earthquake Engineering Research; 2012.

16. H. Öry, E. Wilczek (1983): "Stress and stiffness calculation of thin-walled curved pipes with realistic boundary conditions being loaded in the plane of curvature", Int J Pressure Vessels Piping, 12, pp. 167–189.

17. Rajeev P, Kodikara J. Numerical analysis of an experimental pipe buried in swelling soil. Comput Geotech 2011;38:897–904. doi:10.1016/j.compgeo.2011.06.005.

18. K. Thomas (1981): "Stiffening effects on thin-walled piping elbows of adjacent piping and nozzle constraints", Pressure Vessels Piping Div ASME, 50 (1981), pp. 93–108.

19. Trifonov, O.V., Cherniy, V.P. 2010. A semi-analytical approach to a nonlinear stress-strain analysis of buried steel pipelines crossing active faults, Soil Dynamics and Earthquake Engineering 30 (11), 1298-1308.

20. Trifonov, O.V., Cherniy, V.P. 2012. Elastoplastic stress-strain analysis of buried steel pipelines subjected to fault displacements with account for service loads, Soil Dynamics and Earthquake Engineering 33 (1), 54-62.

21. Vazouras, P., Karamanos, S.A., Dakoulas, P. 2012. Mechanical behavior of buried steel pipes crossing active strike-slip faults, Soil Dynamics and Earthquake Engineering 41, 164-180.

22. Vorster TE, Klar A, Soga K, Mair RJ. Estimating the Effects of Tunneling on Existing Pipelines. J Geotech Geoenvironmental Eng 2005;131:1399–410. doi:10.1061/(ASCE)1090-0241(2005)131:11(1399).

23. WangYu, ShiJiangwei, W.W. N. Numerical modeling of tunneling effect on buried pipelines. Can Geotech J 2011.

24. Wols BA, van Thienen P. Modelling the effect of climate change induced soil settling on drinking water distribution pipes. Comput Geotech 2014;55:240–7. doi:10.1016/j.compgeo.2013.09.003.

25. Xie X., Symans M. D., O'Rourke M. J., Abdoun T. H., O'Rourke T. D., Palmer M. C. & Stewart H. E. 2011. Numerical modeling of buried HDPE Pipelines subjected to strike-slip faulting, Journal of Earthquake Engineering 15, 1273–1296.

Tables

Table 1. API5L-X65 steel properties considered in the parametric analyses.

Yield stress (σ_1)	490 MPa
Yield strain ($\varepsilon_1=\sigma_1/E_1$)	531 MPa
Failure stress (σ_2)	4.0 %
Failure strain (ε_2)	210 GPa
Elastic Young's modulus (E_1)	0.233 %
Plastic Young's modulus ($E_2=(\sigma_2-\sigma_1)/(\varepsilon_2-\varepsilon_1)$)	1.088 GPa

Table 2. Soil spring properties considered in the analyses.

	Yield Force (kN/m)	Yield Displacement (mm)
Axial (friction) springs	40.5	3.0
Transverse horizontal springs	318.6	11.4

Figure captions

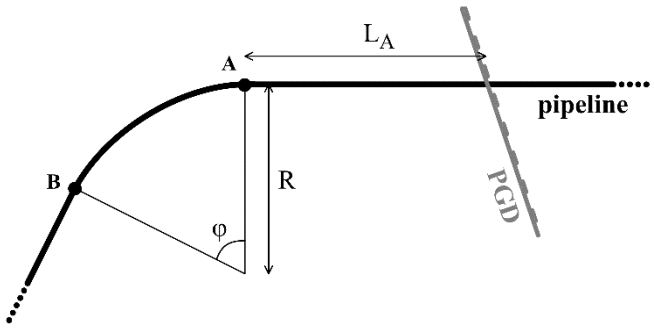

Figure 1. Definition of basic problem parameters.

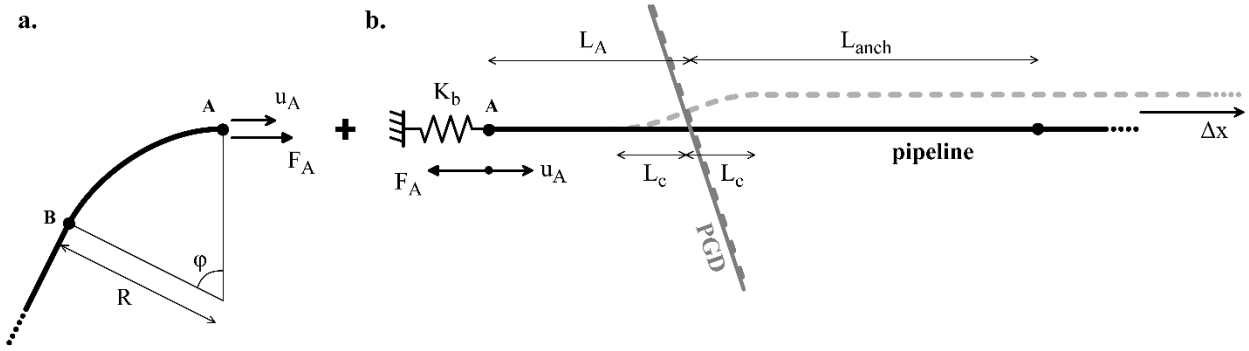

Figure 2. Decomposition of the pipeline into (a) a curved and (b) a straight segment.

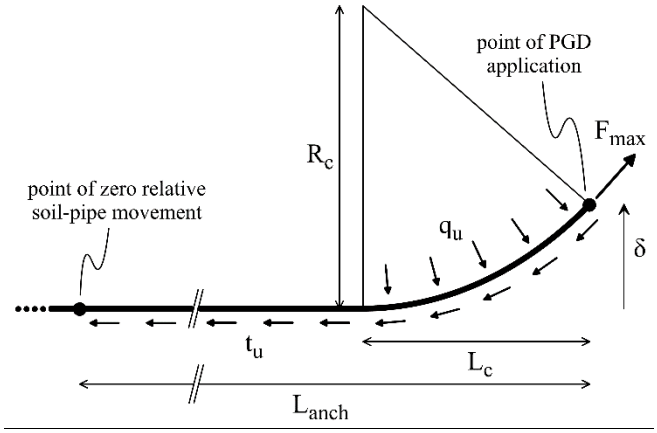

Figure 3. Definition of pipeline curved length L_c and unanchored length L_{anch}.

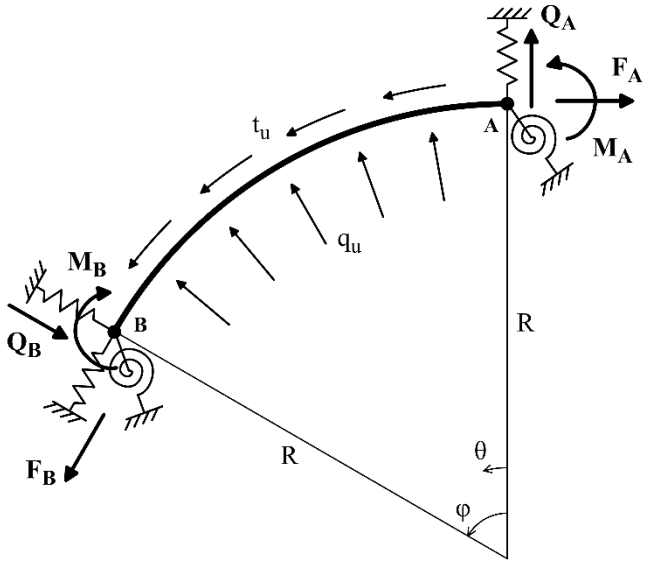

Figure 4. Structural model of the arched pipeline bend.

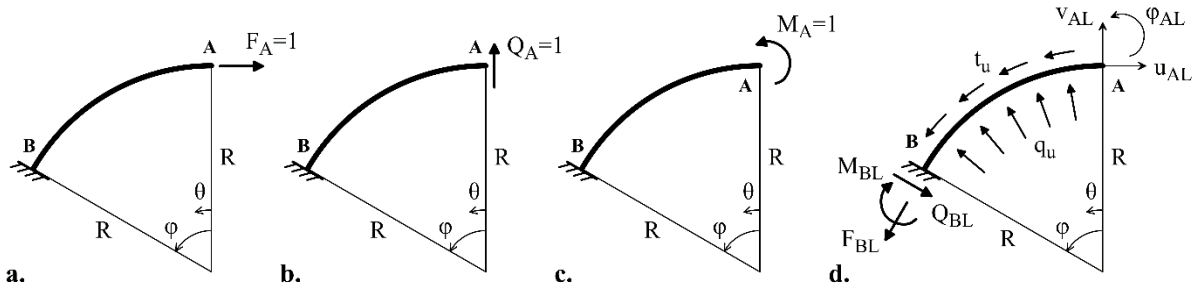

Figure 5. Reduced structure loaded with (a) unit axial force F_A=1, (b) unit shear force Q_A=1, (c) unit moment M_A=1 and (d) soil resistance loads t_u and q_u.

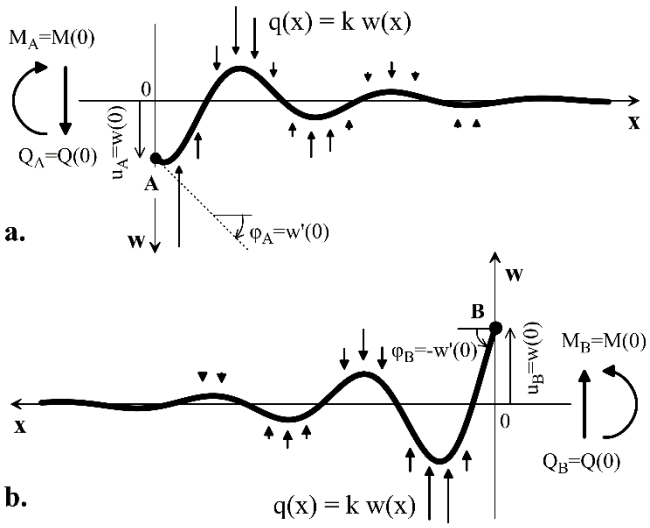

Figure 6. Elastic beam on elastic foundation: boundary conditions for (a) point A and (b) point B.

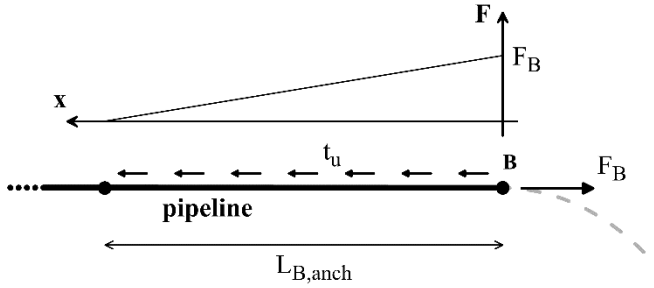

Figure 7. Distribution of axial forces with distance beyond point B.

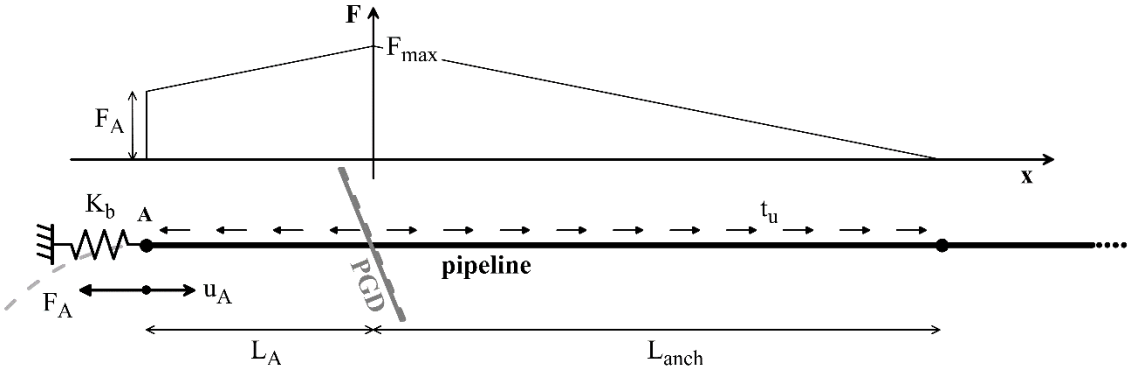

Figure 8. Distribution of axial forces along the straight part of the pipeline.

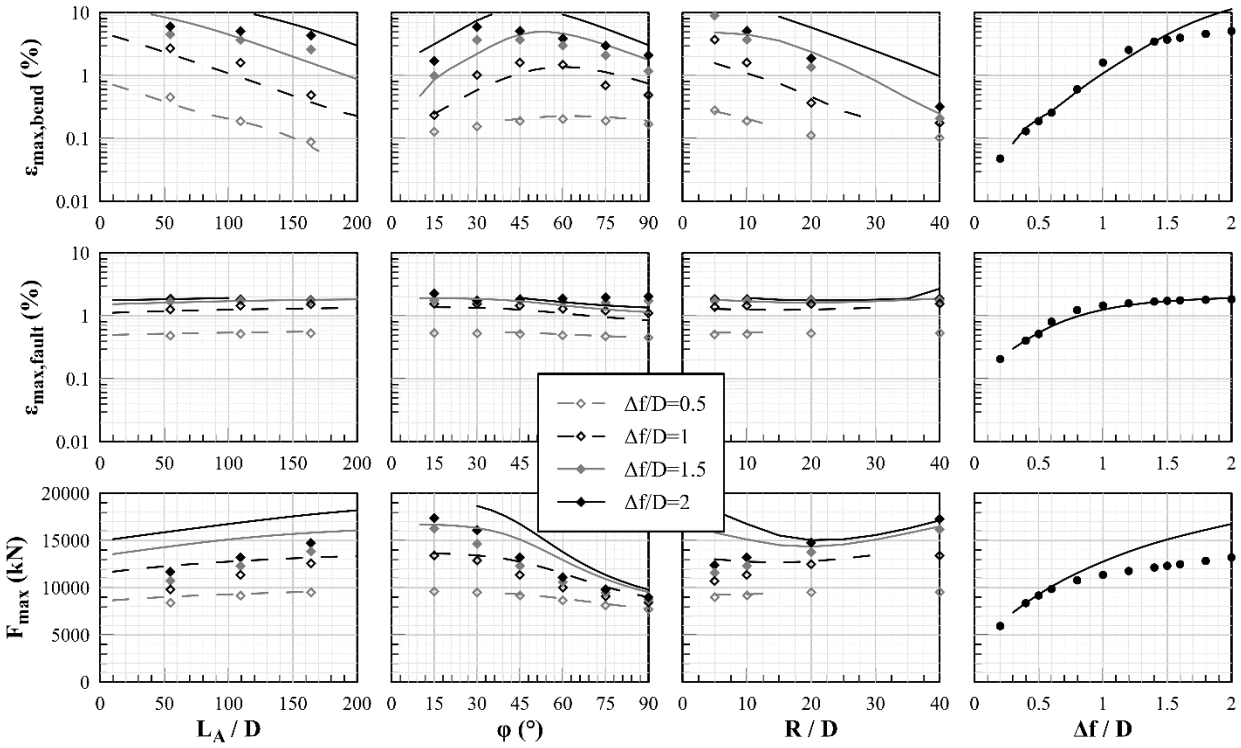

Figure 9. Comparison of analytical predictions (lines) against numerical results (points).

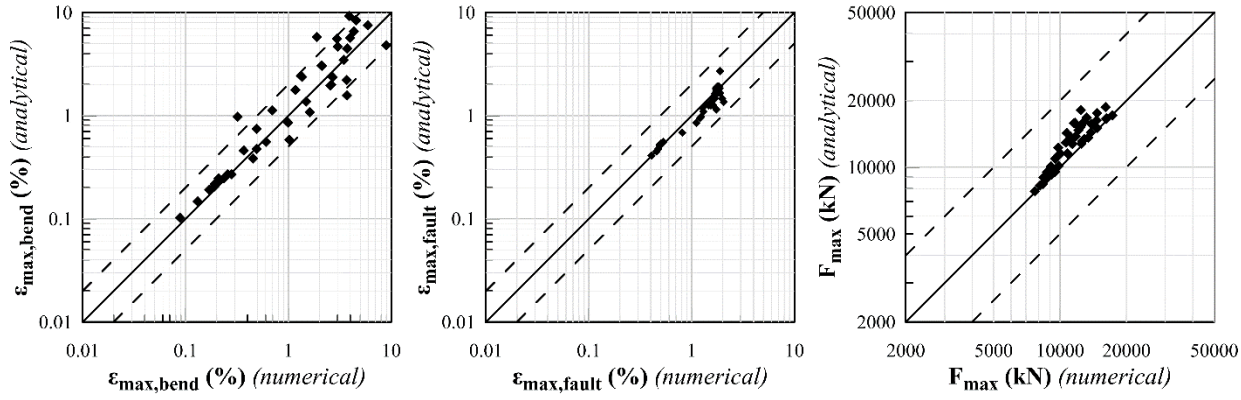

Figure 10. One-to-one comparison of analytical predictions against numerical results.

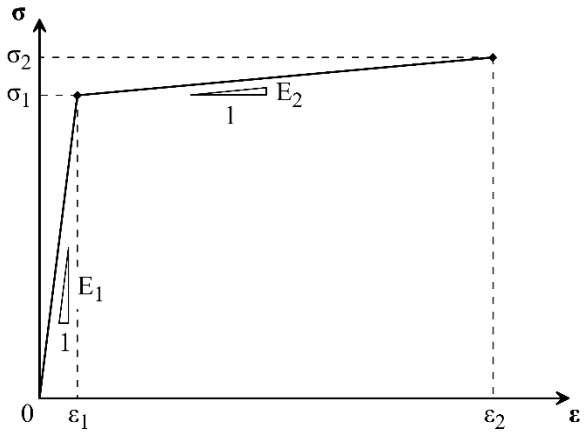

Figure 11. Bi-linear stress-strain relationship of pipeline steel.

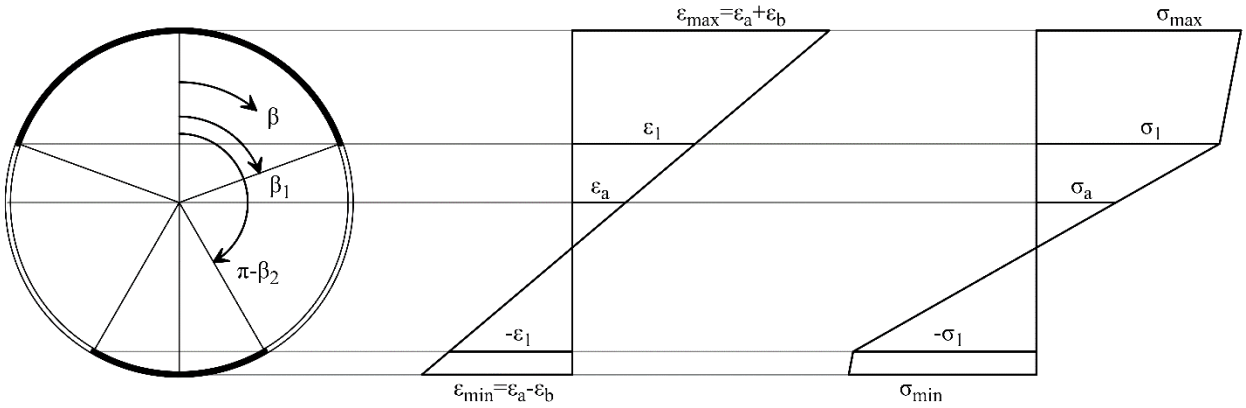

Figure 12. Distribution of stresses and strains over the pipeline's cross-section.

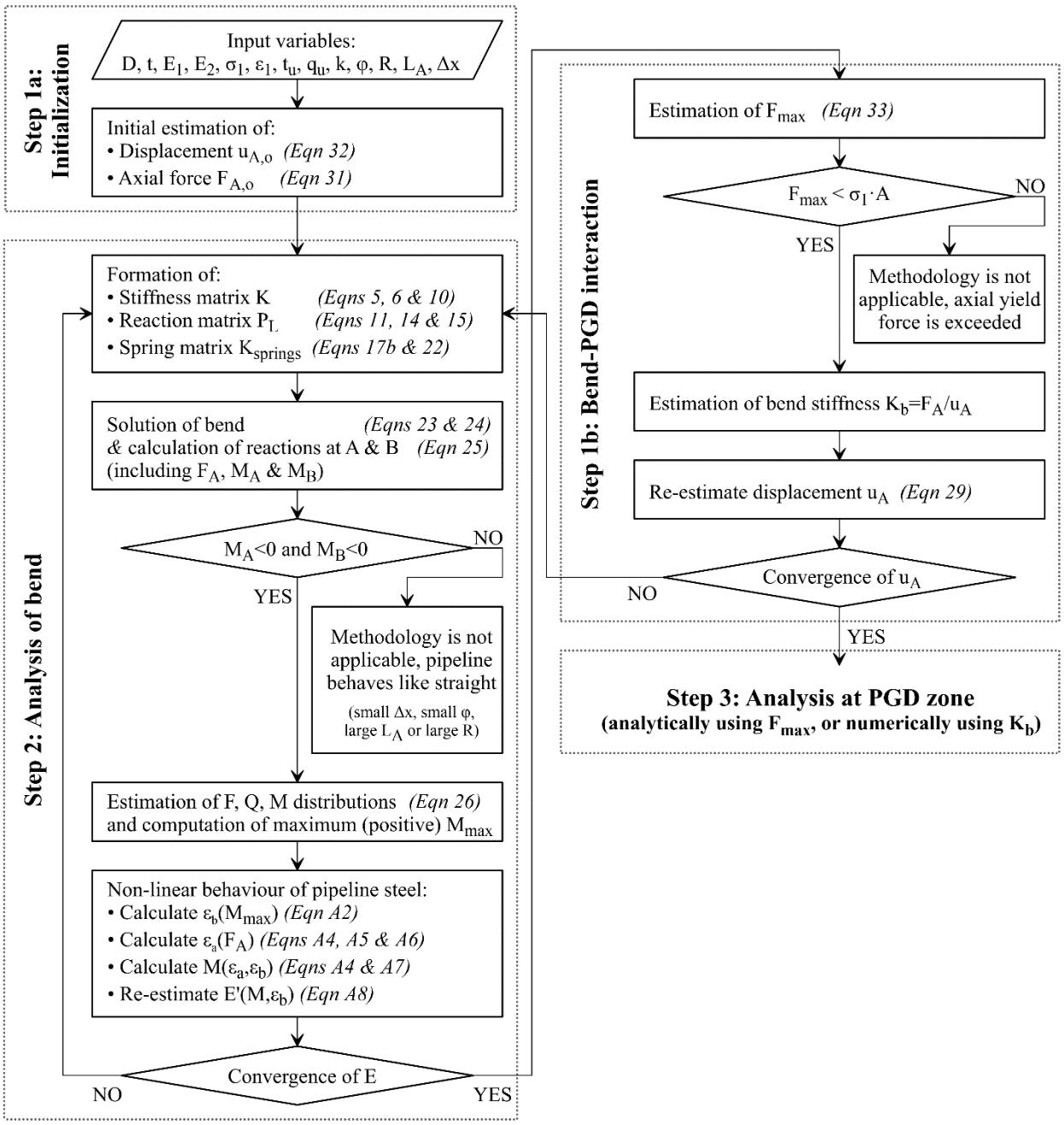

Figure 13. Proposed methodology workflow.